

Discovery of Tidal Tails in Disrupting Open Clusters: Coma Berenices and a Neighbor Stellar Group

SHIH-YUN TANG,¹ XIAOYING PANG*,^{2,3,4} ZHEN YUAN,⁵ W. P. CHEN,^{6,1} JONGSUK HONG,⁷ BERTRAND GOLDMAN,^{8,9}
ANDREAS JUST,¹⁰ BEKDAULET SHUKIRGALIYEV,^{10,11,12} AND CHIEN-CHENG LIN^{8,13}

¹*Department of Physics, National Central University, 300 Zhongda Road, Zhongli, Taoyuan 32001, Taiwan*

²*Xi'an Jiaotong-Liverpool University, 111 Ren'ai Road, Dushu Lake Science and Education Innovation District, Suzhou 215123, Jiangsu Province, P. R. China. Xiaoying.Pang@xjtlu.edu.cn*

³*Shanghai Institute of Technology, 100 Haiquan Road, Fengxian district, Shanghai 201418, P.R. China.*

⁴*Shanghai Key Laboratory for Astrophysics, Shanghai Normal University, 100 Guilin Road, Shanghai 200234, P.R. China*

⁵*Key Laboratory for Research in Galaxies and Cosmology, Shanghai Astronomical Observatory, Chinese Academy of Sciences, 80 Nandan Road, Shanghai 200030, P.R. China*

⁶*Graduate Institute of Astronomy, National Central University, 300 Zhongda Road, Zhongli, Taoyuan 32001, Taiwan*

⁷*Kavli Institute for Astronomy and Astrophysics, Peking University, Yi He Yuan Lu 5, HaiDian District, Beijing 100871, P.R. China*

⁸*Max Planck Institute for Astronomy, Königstuhl 17, D-69117 Heidelberg, Germany*

⁹*Observatoire astronomique de Strasbourg, Université de Strasbourg - CNRS UMR 7550, 11 rue de l'Université, 67000, Strasbourg, France*

¹⁰*Zentrum für Astronomie der Universität Heidelberg, Astronomisches Rechen-Institut, Mönchhofstr. 12-14, 69120 Heidelberg, Germany*

¹¹*Fesenkov Astrophysical Institute, Observatory str. 23, 050020 Almaty, Kazakhstan*

¹²*Faculty of Physics and Technology, Al-Farabi Kazakh National University, Al-Farabi ave. 71, 050040 Almaty, Kazakhstan*

¹³*Institute for Astronomy, University of Hawaii, 2680 Woodlawn Drive, Honolulu, HI 96822, USA*

(Received February 2, 2019; Revised March 2, 2019; Accepted March 27, 2019)

Submitted to ApJ

ABSTRACT

We report the discovery of tidal structures around the intermediate-aged ($\sim 700\text{--}800$ Myr), nearby (~ 85 pc) star cluster Coma Berenices. The spatial and kinematic grouping of stars is determined with the *Gaia* DR2 parallax and proper motion data, by a clustering analysis tool, STARGO, to map 5D parameters ($X, Y, Z, \mu_\alpha \cos \delta, \mu_\delta$) onto a 2D neural network. A leading and a trailing tails, each with an extension of ~ 50 pc are revealed for the first time around this disrupting star cluster. The cluster members, totaling to $\sim 115_{-3}^{+5} M_\odot$, are clearly mass segregated, and exhibit a flat mass function with $\alpha \sim 0.79 \pm 0.16$, in the sense of $dN/dm \propto m^{-\alpha}$, where N is the number of member stars and m is stellar mass, in the mass range of $m = 0.25\text{--}2.51 M_\odot$. Within the tidal radius of ~ 6.9 pc, there are 77 member candidates with an average position, i.e., as the cluster center, of R.A. = 186.8110 deg, and decl. = 25.8112 deg, and an average distance of 85.8 pc. Additional 120 member candidates reside in the tidal structures, i.e., outnumbering those in the cluster core. The expansion of escaping members lead to an anisotropy in the velocity field of the tidal tails. Our analysis also serendipitously uncovers an adjacent stellar group, part of which has been cataloged in the literature. We identify 218 member candidates, 10 times more than previously known. This star group is some 65 pc away from, and ~ 400 Myr younger than, Coma Ber, but is already at the final stage of disruption.

Keywords: stars: evolution — open clusters and associations: individual (Coma Berenices) – stars: kinematics and dynamic

1. INTRODUCTION

Stars are born in dense molecular clouds, and those that remain gravitationally bound appear as star clusters (Lada & Lada 2003). Stars inside a cluster interact with each other via two-body relaxation. As a consequence, massive members slow down and sink to the cluster center, where low-mass stars speed up occupy-

ing a larger column progressively and eventually escape. The so-called “mass segregation” is often observed in star clusters (Hillenbrand & Hartmann 1998; Pang et al. 2013; Tang et al. 2018). In the meanwhile, Galactic potential perturbs star clusters leading to the formation of tidal structures. For example, giant tidal tails have

been found in the isolated halo globular cluster Palomar 5 (Odenkirchen et al. 2001, 2003).

The Galactic disk is abundant in stars, spiral arms, and giant molecular clouds. Therefore, star clusters located in the disk are subjected to disturbance, such as disk shock, spiral arm passage, molecular cloud encounters, etc. (Spitzer 1958; Kruijssen 2012). The typical survival timescale of open clusters in the Galactic disk is about 200 Myr (Bonatto et al. 2006; Yang et al. 2013). Open clusters much older than the survival timescale must have their shape distorted, and structure loosened, leading to inevitable disruption. The disintegrated open clusters become moving groups and then supply field stars. A small portion of these stellar group remnants can be identified by convergent-point method (Boss 1908) in the solar neighborhood (such as the TW Hydrae association, AB doradus moving group and more; Zuckerman & Song 2004).

However, detection of tidally disrupted substructures of open clusters is painstaking. The low number density of a tidal tail may cause its members to be buried in the dense foreground and background field stars. Accurate kinematic data are essential to recover such substructures. *Gaia* data revolutionize this study by providing high precision proper motion (PM) and parallax (ϖ) for nearby open clusters (e.g., Cantat-Gaudin et al. 2018). Based on the 3D motions from *Gaia* TGAS catalog, Oh et al. (2017) identified more than 4555 moving groups in the solar neighborhood. However, only 61 of them have members more than 5, among them, ten are related to known associations. The second data release (DR2) of *Gaia* (Gaia Collaboration et al. 2018) with a higher accuracy on kinematic data, makes it possible to directly reveal tidal tails, e.g., in the nearest open cluster, Hyades (Röser et al. 2019; Meingast & Alves 2019).

The open cluster Coma Berenices (Melotte 111, hereafter Coma Ber) with an age around 800 Myr (Tang et al. 2018) is the second nearest (86.7 pc; Tang et al. 2018) star cluster to the Sun. However, with a large sky coverage and an average PM with no significant difference from that of the field stars, Coma Ber has gotten less attention compared to other nearby clusters. The earliest studies on Coma Ber can be dated back to Melotte (1915) and Trumpler (1938). Later on, Odenkirchen et al. (1998) used the *Hipparcos* and *Tycho* plus the ACT Reference Catalog (Urban et al. 1998), to perform, for the first time, a detailed study with parallax information of Coma Ber, and found a core-halo structure with the major axis parallel to the direction of the Galactic orbital motion of the cluster. They also detected a group of stars with a tangential distance > 10 pc from the cluster center, which they called the “moving group”

of Coma Ber. By studying the luminosity function, they found more faint stars in the moving group than in the central cluster, therefore concluded that Coma Ber was under the process of dissolution. Similar conclusion was given in the later studies by Casewell et al. (2006), Kraus & Hillenbrand (2007), and Tang et al. (2018).

Using the data from *Gaia* DR 2, we explore the neighborhood of Coma Ber and search for tidal tail substructures. In Section 2, we introduce the quality and limitation of the *Gaia* DR 2 data, and explain our input dataset for structure identification. We then present the algorithm, STARGO, which is used to identify structures. The results are shown in Section 3. The dynamical status of Coma Ber and the nearby associated structures, Group-X is discussed in Section 4. Finally, we provide a brief summary in Section 5.

2. DATA AND ANALYSIS

2.1. *Gaia* DR 2 Photometry and Kinematics

As the successor to the *Hipparcos* telescope, *Gaia* is an on-going space mission carried out by the European Space Agency, aiming at providing a detailed three dimensional map on positions and space motions of about one billion stars in our Galaxy and beyond. The DR2 of *Gaia* (Gaia Collaboration et al. 2018) has provided approximately 1.7 billion sources with the celestial positions (R.A. and decl.), and the *G* band (330–1050 nm) photometry, whose magnitude ranges from ~ 3 to 21 mag. Additionally, two other broad-band photometry, G_{BP} (330–680 nm) and G_{RP} (630–1050 nm) are available for around 1.4 billion sources for the very first time.

The astrometry solutions in DR2 have much higher precisions compared to DR1 because they are derived from data collected in a longer time span (22 August 2014 to 23 May 2016) of the nominal mission lifetime. Parallaxes and PMs ($\mu_\alpha \cos \delta, \mu_\delta$) are available for about 1.3 billion sources. The median uncertainty of ϖ without considering the systematic errors is ~ 0.04 mas for bright sources with $G < 14$ mag, 0.1 mas for $G \approx 17$ mag, and ~ 0.7 mas for $G \approx 20$ mag. The corresponding uncertainties of PMs (without considering the systematic errors) for these sources are 0.05, 0.2 and 1.2 mas yr $^{-1}$, respectively (Lindgren et al. 2018).

The RV spectrometer on the *Gaia* telescope collects spectra with a medium resolution ($R \sim 11700$) in the wavelength range of 845–872 nm, centering at the calcium triplet region. However, the radial velocity (RV) in DR2 is only available for bright sources (~ 7.2 million stars), with a typical uncertainty less than 2 km s $^{-1}$ (Gaia Collaboration et al. 2018).

2.2. Input Data

The N-body simulation of [Ernst et al. \(2011\)](#) has shown that tidal tails of an open cluster can be as long as 800 pc, with a core region less than 100 pc (Figure 6 in [Ernst et al. \(2011\)](#)). However, this is likely an upper limit since the simulation only considered Galactic potential as the tidal source, without external perturbations such as molecular cloud interaction, disk shocking, or spiral arm passages. Conceivably, only the most inner part of tidal tails close to the cluster center can be preserved. In this work, we search for tidal tails around the Coma Ber within a radius of 85 pc of its center. Here, we take the distance of Coma Ber as 86.7 pc ([Tang et al. 2018](#)), and the equatorial coordinates of its center as (R.A.=12^h25^m, decl.=26°06′, J2000) from [Dias et al. \(2014\)](#). From the above, the Cartesian Galactocentric coordinates of the cluster center is $(X, Y, Z) = (-8304.9, -5.9, +112.1)$ pc.

To exclude possible artifacts in *Gaia* DR2, we apply the astrometric quality cuts: $\varpi/\Delta\varpi > 10$, and the “astrometric excess noise” < 1 mas, suggested by [Lindgren et al. \(2018\)](#) (in their Appendix C). Furthermore, we only use RV data with errors < 1 km s⁻¹. The final “cleaned” sample contains 152,739 sources which we call Sample I. This sample has the *G* magnitudes ranging from ~ 3.2 mag to ~ 20.7 mag, with the distribution function turning around, i.e., being significantly incomplete, beyond ~ 16 mag, as shown in Figure 1 (a). About 25 percent of the sources in Sample I have available RV. Figure 2 (a) shows the PM vector plot of Sample I around Coma Ber. Interestingly, an additional belt-like over-density is seen. In Figure 2 (b), the belt-like feature reveals itself robustly on a 2D density map that only shows bins with an over-density $> 5\sigma$. To include this belt-like structure and Coma Ber, we apply a cut in PMs, $\mu_\alpha \cos \delta$ between -25 and 0 mas yr⁻¹ and μ_δ between -15 and 10 mas yr⁻¹ (the black box in Figure 2 (b)). This reduces the number of stars to 5,494, which is called Sample II. This sample is very similar to Sample I with magnitudes ranging from ~ 3.0 mag to ~ 20.8 mag, and complete near ~ 16.5 mag (see Figure 1 (b)).

In this study, we use 5D parameters of stars in Sample II (R.A., decl., ϖ , $\mu_\alpha \cos \delta$, and μ_δ) from *Gaia* DR2. Since only a fraction of stars (~ 23 percent) have RV measurements, RV is used supplementarily. Stars in Sample II are all located within 175 pc from the Sun, which makes the most probable distance of each star very close to the inverse of ϖ ([Bailer-Jones et al. 2018](#)). Therefore, adopting $1/\varpi$ as the distance, we compute for each source the Galactocentric Cartesian coordinates (X, Y, Z) . The transformation is performed by using the

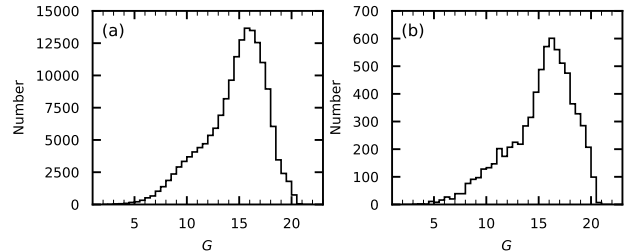


Figure 1. Number of *Gaia* DR2 stars in *G* band of Sample I is shown in (a), and Sample II shown in (b).

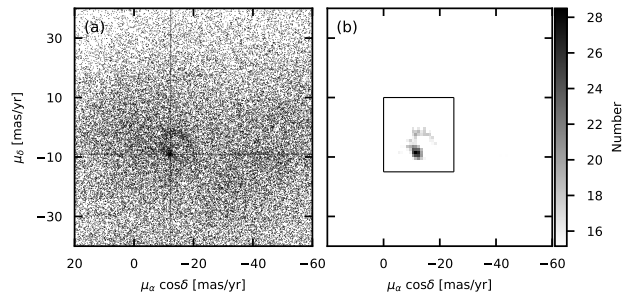


Figure 2. (a) Proper motion vector plot for sample I around Coma Ber, which generates an over-density as the cross indicated. (b) 2D density map for sample I. Each bin is smoothed by neighboring 8 bins and here only bins with a number count > 12.8 (5σ , where σ is the standard deviation of all bins) are shown. The black box indicates the PM ranges of Sample II.

Python *Astropy* package ([Astropy Collaboration et al. 2013, 2018](#)). Assumptions used in the conversion, such as the solar position and its Galactic velocities are listed in Appendix A.

2.3. Structure Identification with STARGO

We use a novel cluster finding method STARGO ([Yuan et al. 2018](#)) to search for tail structures around Coma Ber. Our method is built with self-organizing map (SOM), which is one of the well-established unsupervised learning algorithms based on artificial neural network. The goal of SOM is to create a network that stores the information in such a way that the topological structures of the input data are preserved. Based on that, structures having grouping signature in the input space will be more easy to be identified.

An open cluster is a group of stars formed from the same giant molecular cloud. Before the member stars are fully dissolved, they are clustered in the phase space. In this work, we apply STARGO to the stellar sample around Coma Ber in the 5D space of $(X, Y, Z, \mu_\alpha \cos \delta, \mu_\delta)$. The unsupervised learning of the neural network is performed as follows.

1. We generate a 2D network with 100×100 neurons located at different grid points. The distances between neurons are defined as the Euclidean distances on the 2D map. Each neuron is assigned with a 5D weight vector which has the same dimension as the input space.
2. From the sample, we pick one star and find the neuron with the closest weight vector to its input vector, which is defined as the best matching unit (BMU). Each neuron updates its weight vector according to its distance to the BMU. The learning algorithm enforces the neurons, that located further from the BMU on the map, get less affected by the input star.
3. Stars are fed to the neural network one by one, where all the neurons keep updating their weight vectors from the previous values. One iteration is complete after the neurons learn the behavior from all the stars of the sample once. The whole learning process is iterated by 400 times when the weight vectors reach convergence. We associate all the stars from our sample to the final map with their BMUs.

The differences in weight vectors between adjacent neurons are denoted by a matrix, u . The trained neural network can be visualized by the gray scale map of u (as illustrated in Figure 3 (b)). The lighter gray shaded neurons have smaller u , which means that their weight vectors are more similar to their neighbors compared to the darker shaded ones. Thus the stars associated with the former are closer in the input space. As we can see clearly from Figure 3 (b), the lighter shaded neurons form two distinctive patches. These neurons have significantly lower values of u than the others, which are supposed to be associated with the stars clustered in the input space. Consistently, we see an extended tail on the left side of the distribution of u in Figure 3 (a), indicating that there are some neurons with significant low values of u . We take the following steps to select these neurons. Firstly, we find the peak position u_{peak} and the 99.85th percentile of the distribution $u_{99.85\%}$, which are denoted by the dotted lines respectively in Figure 3 (a). The quantity $u_{99.85\%} - u_{\text{peak}}$ is equivalent to 3σ of a normal distribution, which is denoted as $\Delta_{3\sigma}$. We then define the left tail of this distribution by $u_{\text{peak}-3\sigma} < u_{\text{peak}} - \Delta_{3\sigma}$, shown as the cyan shaded region in Figure 3 (a). We mark all the neurons with $u \leq u_{\text{peak}-3\sigma}$ by cyan in Figure 3 (c), and color the two most major groups of 197 and 218 stars in red and blue, respectively. These two groups correspond to Coma Ber

and its nearby group (here and after group-X), which will be discussed in detail in Section 3.

2.4. Uncertainty and Contamination

The observational uncertainties are taken into account by using the trained 2D neuron map. We first compute the difference between the input vector of each star and its BMUs, denoted by u_{vw} . The maximum difference from the training sample is quantified as $u_{\text{vw,max}}$, which denotes the limit of the neuron map. For each member candidate of the identified group, we create 1000 realizations which follow the Gaussian distribution in each dimension of $(\varpi, \mu_\alpha \cos \delta, \mu_\delta)$ with the observed value as the mean and the uncertainty as the covariance. We find BMU for each mock realization star from the trained map. We then calculate the difference between the input vector of the mock star and its associated BMU. For stars with large observational errors, the mock realizations may have u_{vw} larger than $u_{\text{vw,max}}$. We remove those stars since they cannot be tightly associated with the trained neuron map. For each candidate members, more than 900 out of 1000 of its mock realization attach to the corresponding group. In another word, the probability to recover member candidates is more than 90%, considering observed uncertainties.

We then evaluate the contamination fraction from the smooth Galactic disk background using the mock *Gaia* DR2 catalog of Rybizki et al. (2018), which is based on the *Galaxia/Besançon* models (Sharma et al. 2011; Robin et al. 2011). The same cut on ϖ and PM as per Section. 2.2 were exerted on the mock catalog in the same volume of the sky (within 85 pc around the center of Coma Ber). There are 3,494 and 592 mock stars within the sky area of the two identified clusters, respectively. Following the recipe described in the previous section, we attach each of these mock stars with the trained map, and find 20 stars associated with Coma Ber and 12 stars associated with group-X. Therefore, the mock smooth background gives $20/3,494 = 0.6\%$ of field stars in the region of Coma Ber, and $12/592 = 2\%$ in the region of group-X. Considering the observed stars within the sky area of the two identified clusters (1,794 and 658), the contamination fraction estimated from the mock data is 5%–6% (Coma Ber: $1,794 \times 0.6\%/197$; group-X: $658 \times 2\%/218$).

We also verify the choice of the searching volume for cluster identification by enlarging the radius to 100 pc and 150 pc. In either case, similar member lists of the targeted open clusters are obtained. We do not find significantly extended structures beyond 85 pc for these two clusters. Therefore in this paper, we only present the results within the fiducial volume.

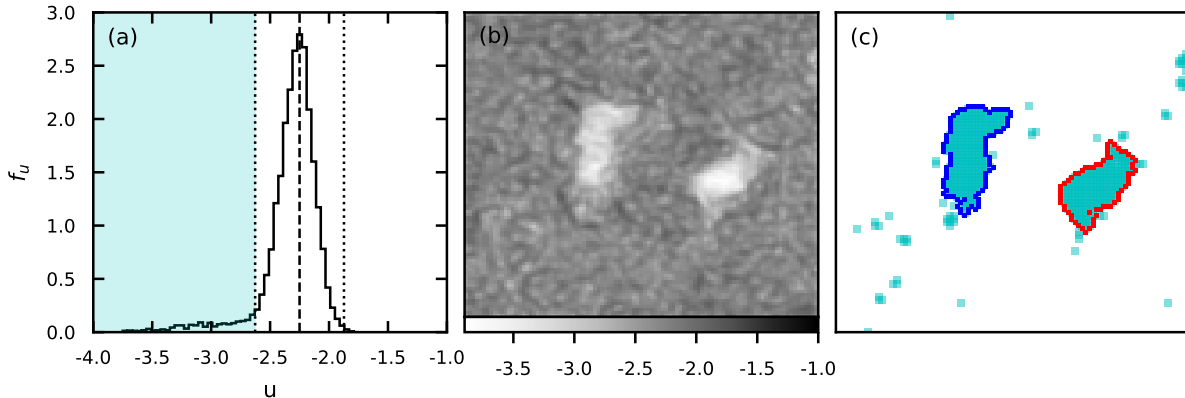


Figure 3. Group identified by applying STARGO to the data sample in the $(X, Y, Z, \mu_\alpha \cos \delta, \mu_\delta)$ space. (a) histogram shows the distribution of u . The dashed line denotes the peak position of its distribution u_{peak} and the dotted lines show $u_{\text{peak}-3\sigma}$ and $u_{\text{peak}+3\sigma}$, respectively. The left tail with $u < u_{\text{peak}-3\sigma}$ is highlighted in cyan. (b) 2D neural map resulting from SOM, where the u value between adjacent neurons is represented by the gray-scale. (c) is the same as (b) where the neurons with $u < u_{\text{peak}-3\sigma}$ are colored in cyan. Contours of two dominant neuron groups are traced with different colors (red: Coma Ber; blue: group-X).

3. IDENTIFIED STRUCTURES

3.1. *Coma Ber and its Tidal Tail*

In Figure 4 (a) and (b), we show the 3D spatial distributions of Coma Ber member candidates in Table 1, with the running number (column 1), the astrometric (position, ϖ and PM) and photometric (magnitude) information from *Gaia* DR 2 listed in column 2 to 12. The cluster is already known to be elongated along the Z axis Tang et al. (2018) with most of the extended members fainter than the brightness limit of *Gaia* DR 2. In this study, we find the elongation on the X–Y plane, leading to an overall morphology of an ellipsoid.

The differential gravitational force of the Milky Way, i.e., the Galactic tide, acts to stretch objects such as open clusters (Martinez-Medina et al. 2017). The Galactic tide is extensive along the radial direction, and compressive along the vertical direction of the plane (Spitzer 1987), thereby re-shaping open clusters into an ellipsoid. Stars in an ellipsoid have different Galactocentric distances. Due to the differential rotation, stars closer to the Galactic center rotate faster.

Therefore, one part of the ellipsoid is leading while the other is trailing. This is what is seen in the morphology of Coma Ber, shown in Figure 4 (a) and (c), and is discovered for the first time for this star cluster.

We show the orbit motion of Coma Ber with a grey arrow in panels (a) and (b). The orbit is computed base on the average position of Coma Ber (Section 2.2) and its median velocity, by the Python galpy package (Bovy 2015) with the Galactic potential,

“MWPotential2014¹”. Orbits are integrated 0.5 Myr backward and 1 Myr forward in time.

Figure 4 (c) is the same as Figure 4 (a) but with the color coding and symbol size scaled to the absolute G magnitude (M_G). As can be seen, brighter stars are concentrated toward the center, which confirms the mass segregation previously known in Coma Ber (Odenkirchen et al. 1998; Casewell et al. 2006; Kraus & Hillenbrand 2007; Tang et al. 2018). Compared to the local standard of rest (LSR; Kerr & Lynden-Bell 1986) the extension of tidal tails are aligned with the major axis of the ellipsoid of Coma Ber indicated by the grey big arrow in Figure 4 (c), which is the projection of mean velocity vector of Coma Ber $(U, V, W) = (8.6, 226.6, 6.8)$ km s⁻¹ relative to LSR: $(U, V - 220, W) = (8.6, 6.6, 6.8)$ km s⁻¹.

A recent work by Tang et al. (2018) has carried out a comprehensive study on Coma Ber within a 5° radius sky area for stars from the bright end ($J \sim 3$ mag $\sim 2.3 M_\odot$) down to the brown dwarf regime ($J \sim 17.5$ mag $\sim 0.06 M_\odot$). For member candidates outside the 5° radius, they had collected from other studies (Trumpler 1938; Casewell et al. 2006; Kraus & Hillenbrand 2007; Mermilliod et al. 2008; Melnikov & Eisloffel 2012; Gaia Collaboration et al. 2017) if the candidate also satisfied Tang et al. (2018)’s selection criteria. Among their 154 bright members, our candidate list (red dots in Figure 4) recovers 82 stars (dark red open

¹ MWPotential2014 is a Galactic potential model made of three components, the bulge, disk, and halo. Parameters of the model were fitted to published dynamical data of the Milky Way.

circles in Figure 4 (a) and (b)), which are located in the cluster center. The others might be field star contamination since Tang et al. (2018) applied a large radius cut (17 mas yr^{-1}) on PM selection (see their Figure 4) compared to the very concentrated PM of our member candidates (see Figure 4 (d)) with standard deviations of $\sigma_{\mu_{\alpha} \cos \delta} = 1.2 \text{ mas yr}^{-1}$ and $\sigma_{\mu_{\delta}} = 1.2 \text{ mas yr}^{-1}$.

Five stars identified by Odenkirchen et al. (1998), HD 114400, BD+21 2514, BD+38 2436, HD 116706, and BD+26 2461, were called as Coma Ber’s moving group. They are recovered by the STARGO algorithm as Coma Ber’s member candidates (see green open circles in Figure 4 (a) and (b)). These five stars are indeed located further away from the main cluster, belonging to the tidal tail structures.

3.2. Group-X

Although Coma Ber and the group-X contain similar numbers of stars, they are distinct from each other in the PM vector diagram (Figure 4 (d)). The range of the PM of group-X is wider than that of Coma Ber, with standard deviations of $\sigma_{\mu_{\alpha} \cos \delta} = 2.6 \text{ mas yr}^{-1}$ and $\sigma_{\mu_{\delta}} = 2.5 \text{ mas yr}^{-1}$. Besides, we also present the RV distributions for 47 member candidates in Coma Ber and 38 in group-X, which have reliable RV measurements (Figure 4 (e)). The distinction of two separate peaks at -0.5 km s^{-1} (Coma Ber) and -7.0 km s^{-1} (group-X) further confirms the fact that Coma Ber and group-X are two dynamically different systems. The narrow

distributions of RV of both groups suggest that their members are kinematically related.

Despite the proximity of group-X, among the 218 member candidates we identify, 27 were first discovered by Oh et al. (2017) via the ϖ and PMs from *Gaia* DR1 TGAS data. These 27 stars were members of group 10 in Oh et al. (2017)’s Table 1 (hereafter Oh10), and were confirmed as a newly found moving group in Faherty et al. (2018). We plot Oh10’s 27 stars as orange open circles in Figure 4 (a) and (b). They are all bright stars and located in two dense patches, tracing out the shape of the two clumps (most of dark and large circles in group-X in Figure 4 (c)). In addition to Oh10, 3 member candidates of group-X belong to group 81 in Oh et al. (2017) (hereafter Oh81, grey open circles), and two belong to their group 1805 (hereafter Oh1805, pink open circles).

Besides Oh10, Oh81, and Oh1805, the remaining 186 stars are dynamically associated as a group in Figure 4 (d) and (e). The extended distribution of PMs of group-X may reflect the disrupted nature of a moving group for which all members might share the same origin. The member candidates for group-X are listed in Table 2, with columns 2 to 12 presenting the astrometric and photometric data from *Gaia* DR 2 (the same format as Table 1).

Table 1. Coma Ber Member Candidates

No.	R.A.	Decl.	Plx	Plxerr	$\mu_{\alpha} \cos \delta$	$\Delta\mu_{\alpha} \cos \delta$	μ_{δ}	$\Delta\mu_{\delta}$	RV	RVerr	<i>G</i>	flag [†]
	(J2015.5 deg)		(mas)		(mas yr ⁻¹)		(mas yr ⁻¹)		(km s ⁻¹)		(mag)	
(1)	(2)	(3)	(4)	(5)	(6)	(7)	(8)	(9)	(10)	(11)	(12)	(13)
1	183.103668	27.380058	11.67	0.05	-12.19	0.08	-9.41	0.05	0.15	0.27	7.97	b
2	183.178196	25.228414	11.31	0.12	-11.75	0.17	-7.85	0.12	16.52	b
3	183.221756	26.250356	11.59	0.04	-12.07	0.06	-9.52	0.04	0.59	1.01	11.10	b
4	183.881094	25.066959	11.32	0.11	-12.13	0.17	-9.13	0.14	16.04	b
5	184.034840	25.760327	11.72	0.05	-12.23	0.08	-10.53	0.06	2.06	0.37	7.98	b
78	164.212295	17.330554	9.79	0.17	-10.73	0.29	-8.26	0.30	17.18	t
79	165.493305	20.033749	10.28	0.07	-11.03	0.12	-8.92	0.16	15.04	t
80	166.639954	14.234920	10.18	0.04	-10.95	0.07	-9.10	0.06	1.77	0.66	11.38	t
81	168.564244	9.241932	10.27	0.12	-10.87	0.18	-7.36	0.17	16.86	t
82	170.489998	23.773542	11.74	0.13	-12.24	0.22	-11.05	0.20	16.99	t

NOTE— Entries are sorted according to column 2, R.A.. This table is available in its entirety in a machine-readable form in the online journal. Here we only show the first five member candidates in both the bound (within tidal radius) and the tail regions.

[†] b: “bound” member candidates within tidal radius (see Section 4.3), t: “tail” member candidates.

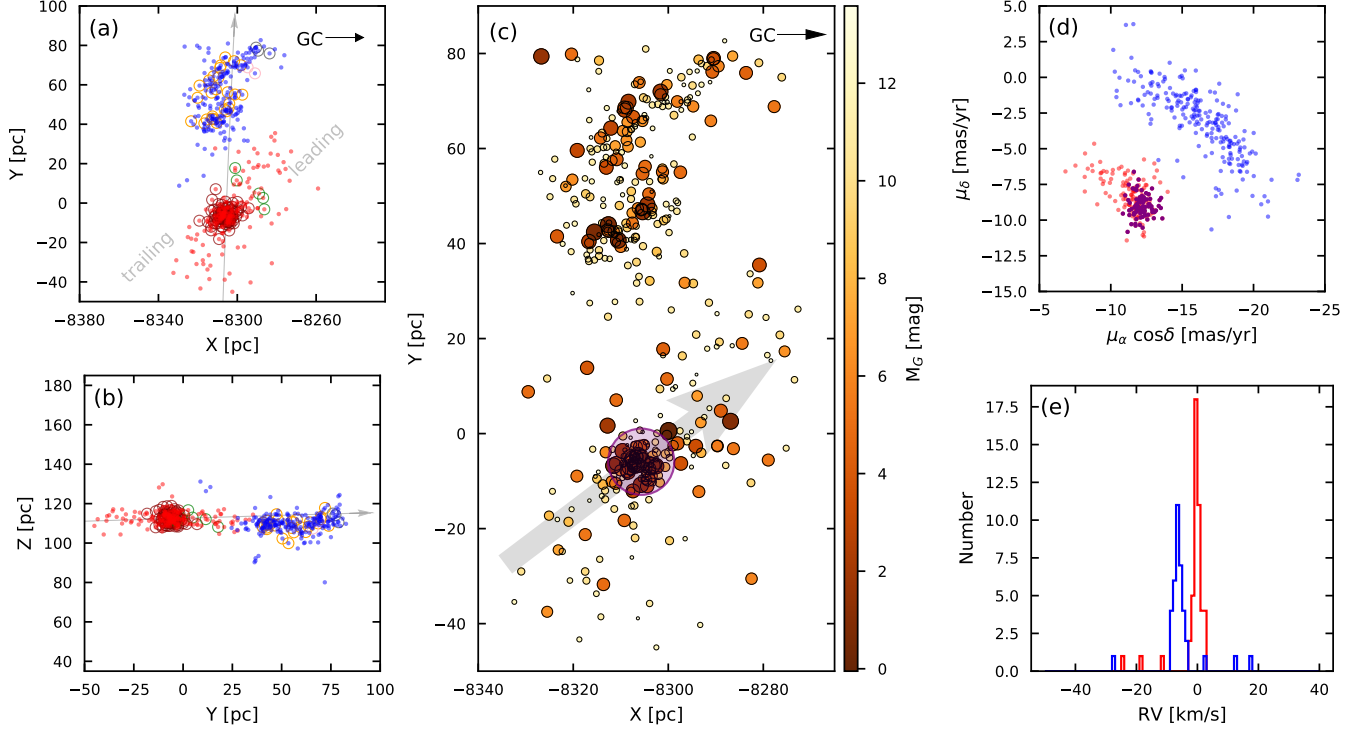


Figure 4. Kinematic and spatial distribution of member candidates (Coma Ber: red; group-X: blue). Members from previous studies are in open circles (Odenkirchen et al. (1998): green; Tang et al. (2018): dark red; Oh et al. (2017)’s group 10: orange; Oh et al. (2017)’s group 81: grey; Oh et al. (2017)’s group 1805: pink). (a) and (b) show the 3D spatial position of member candidates in Galactocentric Cartesian X, Y, Z coordinates. The grey arrow in (a) and (b) is the orbit motion of Coma Ber. (c) is the same as (a), but with the symbols color coded and sizes adjusted to reflect the M_G magnitude. Bright stars are bigger and with darker color. The purple circle shows the region within the tidal radius (6.9 pc, see Section 4.3) of Coma Ber. The big grey arrow is the projected mean velocity vector of Coma Ber relative to LSR. (d) shows the proper motion vector plot with purple dots as the Coma Ber member candidates within the tidal radius. (e) shows the RV histogram.

Table 2. Group-X Member Candidates

No.	R.A.	Decl.	Plx	Plxerr	$\mu_\alpha \cos \delta$	$\Delta\mu_\alpha \cos \delta$	μ_δ	$\Delta\mu_\delta$	RV	RVerr	G
(1)	(J2015.5 deg)	(3)	(4)	(5)	(6)	(7)	(8)	(9)	(10)	(11)	(12)
1	178.948766	39.073363	9.20	0.04	-21.02	0.06	-9.76	0.05	2.88	0.99	10.08
2	181.613107	40.057117	9.69	0.06	-18.27	0.06	-9.78	0.08	15.18
3	187.799135	38.782755	9.64	0.05	-16.22	0.06	-2.35	0.05	17.85	0.24	8.99
4	191.762024	50.574560	11.07	0.15	-19.93	0.19	-8.31	0.21	17.87
5	193.693214	49.169553	11.65	0.06	-20.77	0.07	-8.33	0.08	16.03
6	195.253545	46.072319	11.73	0.05	-20.54	0.06	-8.89	0.06	14.77
7	195.729678	55.236239	10.30	0.08	-18.82	0.11	-7.93	0.12	16.88
8	195.819464	57.315206	10.54	0.03	-17.37	0.04	-8.33	0.04	-3.99	0.90	8.97
9	197.861213	60.205489	12.60	0.07	-21.26	0.10	-7.17	0.10	15.58
10	198.797593	50.390444	10.09	0.07	-15.08	0.09	-7.00	0.09	15.85

NOTE— Entries are sorted according to column 2, R.A.. This table is available in its entirety in a machine-readable form in the online journal. Here we only show the first ten candidates.

4. DISCUSSION

4.1. Cluster Ages

We plot the color-magnitude diagram (CMD) for both groups (Coma Ber: red; group-X: blue) in Figure 5 with stars from Sample I plotted as a density map in the background in Figure 5 (a). There are 25 member candidates

of Coma Ber and 18 of group-X having spectra from the Large Sky Area Multi-Object Fiber Spectroscopy Telescope (LAMOST) DR 4, with $S/N > 40$ in g band (Wu et al. 2014a,b). Both have nearly solar metallicity (Coma Ber to be $[Fe/H] \sim -0.02$ and group-X ~ 0.08), hence we adopt $[Fe/H]=0$ and zero extinction (in the solar neighborhood, Casewell et al. 2006; Tang et al. 2018) for the isochrone, and correct each star for its distance and obtain the CMD in M_G (Figure 5 (b)).

Recent studies (Evans et al. 2018; Weiler 2018; Maíz Apellániz & Weiler 2018) have provided three different sets of the filter response curves for *Gaia* in G , G_{BP} , and G_{RP} bands, thus leading to three different sets of PARSEC isochrones (Bressan et al. 2012; Chen et al. 2014; Tang et al. 2014; Chen et al. 2015), with a large offset (≤ 0.3 mag) in the G_{BP} band for bright stars. Here we adopt the PARSEC isochrones with the sensitivity curves provided by Maíz Apellániz & Weiler (2018) (best match to our data) and plot them in Figure 5 (b). For consistency check, we also present the CMD for bright stars in B and V photometry taken from Tycho-2 catalogue (Høg et al. 2000) in the inset of Figure 5 (b).

The age of Coma Ber is determined by the stars near the main sequence turn-off point, and two stars, 12 Com and 31 Com, just evolving off the main sequence, using the PARSEC isochrone set. Given that 12 Com is a known binary (Griffin & Griffin 2011), hence brighter than a single-star isochrone of the actual age, a range of 700–800 Myr PARSEC isochrone provides the overall best fit. This is consistent with the result of Tang et al. (2018).

The member, WD 1216+260 (in Figure 5 (a)), is spectroscopically confirmed as a DA white dwarf (Dobbie et al. 2009; Girven et al. 2011). According to the cooling time of the white dwarf estimated by Girven et al. (2011), WD 1216+260 must be older than 400 Myr, which sets a lower limit for the age of Coma Ber. This agrees with the age range quoted in the literature.

In contrast, no turn-off stars are present in the CMD of group-X, indicating a younger age. The upper MS of group-X is bluer than Coma Ber, and located very close to the isochrone of 400 Myr in G versus $G_{BP} - G_{RP}$ diagram (Figure 5 (b)). Furthermore, in the B versus $B - V$ diagram, the bright stars clearly line up along the 400 Myr isochrone (inset in Figure 5 (b)). We adopt an age 400 Myr for group-X from isochrone fitting by eye via B and V photometry. Different from our result, Faherty et al. (2018) found a bimodal age distribution by isochrone fitting to individual stars in Oh10, that half of the members are younger than 1 Gyr and the other older than 1 Gyr. Although a WD is found in group-

X (*Gaia* ID, 1648892576918800128, hereafter G164), no study or observations have been carried out on it yet.

4.2. Cluster Mass Function

By adopting an age of 800 Myr for Coma Ber, we estimate the stellar mass for each member by using the PARSEC isochrone, and derive the mass function (MF, Figure 6 (a)). The slope, in a sense of $dN/dm \propto m^{-\alpha}$, is fitted by linear least-squares fitting. In Figure 6 (a), the number of low-mass members of Coma Ber increases by a factor of 5 compared to the study of Tang et al. (2018) at the mass bin of $\sim 0.16 M_{\odot}$. This to be compared with the peak around $0.3 M_{\odot}$ common seen in clusters or associations (Bastian et al. 2010). The slope for present-day MF of Coma Ber ($0.25 M_{\odot}$ to $2.51 M_{\odot}$) is $\alpha \sim 0.79 \pm 0.16$, consistent with that reported by Kraus & Hillenbrand (2007) ($\alpha \sim 0.6 \pm 0.3$ for $0.1 - 1.0 M_{\odot}$). It is flatter than that of group-X with $\alpha \sim 1.19 \pm 0.16$.

We add up the mass of member candidates in Coma Ber to obtain the cluster mass, and correct the incompleteness below $0.2 M_{\odot}$ by adopting the slope ($\alpha \sim -1.69$, black dashed line in Figure 6 (a)) from Tang et al. (2018) since their MF is complete down to $0.08 M_{\odot}$. After integrating the mass lower than $0.2 M_{\odot}$ with $\alpha \sim -1.69$, the mass below the completeness is $6.2 M_{\odot}$. Consequently, the cluster mass of Coma Ber is $115^{+5}_{-3} M_{\odot}$, with the error computed from the uncertainty in the slope of mass function. This is in a good agreement with previous results of $102 - 112 M_{\odot}$ (Casewell et al. 2006; Kraus & Hillenbrand 2007; Tang et al. 2018). The total mass of group-X, after the same completeness correction, is $111^{+16}_{-7} M_{\odot}$ using the PARSEC isochrone of 400 Myr for the mass of each individual member.

4.3. Tidal Radii

The total stellar mass of Coma Ber or group-X approaches the lower limit of open cluster mass, which is around a hundred solar masses (Tadross et al. 2002; Piskunov et al. 2008). However, either system is distributed in a large space volume (Figure 4), ($80 \text{ pc} \times 80 \text{ pc} \times 60 \text{ pc}$) for Coma Ber and ($40 \text{ pc} \times 50 \text{ pc} \times 50 \text{ pc}$) for group-X. That is to say, the low-mass stars located in the tidal tails (especially Coma Ber) probably not be bound to the cluster.

The tidal radius of a system can be computed via

$$r_t = \left(\frac{GM_C}{2(A-B)^2} \right)^{\frac{1}{3}}, \quad (1)$$

(Pinfield et al. 1998) where G is the gravitational constant, M_C is the total mass of the cluster, and A and B are the Oort constants ($A = 15.3 \pm 0.4 \text{ km s}^{-1} \text{ kpc}^{-1}$, $B = -11.9 \pm 0.4 \text{ km s}^{-1} \text{ kpc}^{-1}$; Bovy 2017)

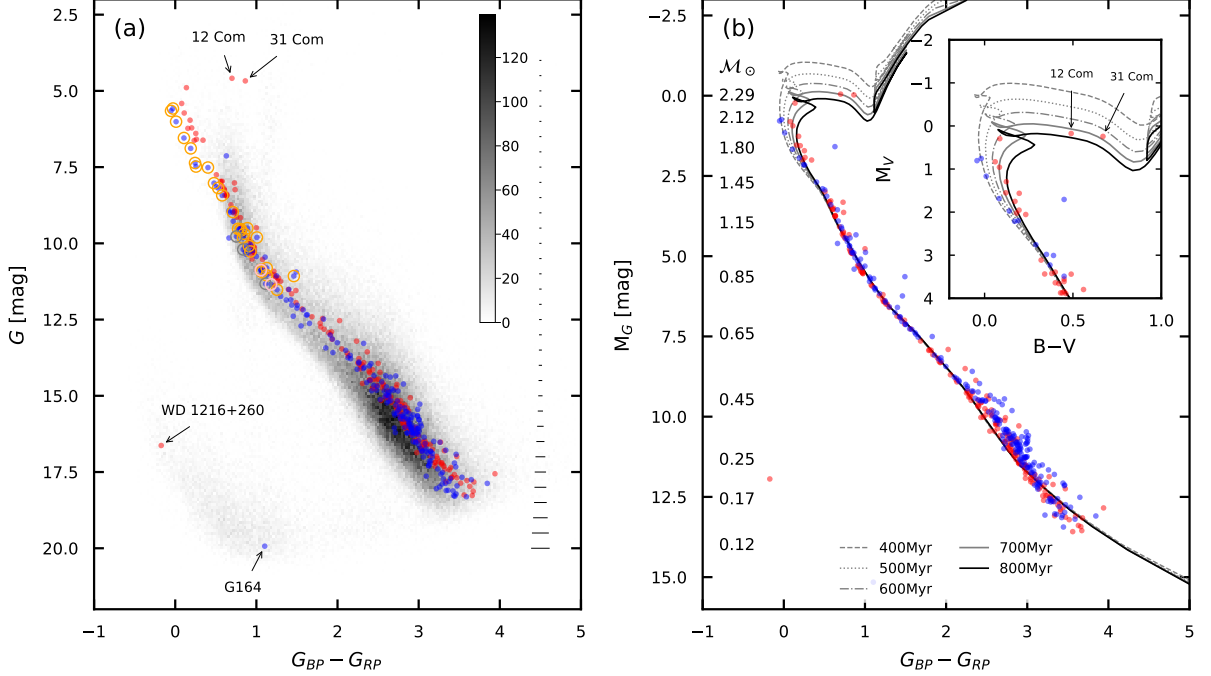


Figure 5. The color-magnitude diagram of (a) *Gaia* apparent G magnitude, and (b) the absolute magnitude M_G (adopting *Gaia* parallax). Symbols are the same as in Figure 4 (a). Objects of Sample-I are shown as a density map in (a). Typical errors in color $G_{BP} - G_{RP}$ are presented as horizontal bars to the right. (b) PARSEC isochrones of 400, 500, 600, 700, and 800 Myr are over-plotted, with zero extinction corrected and solar metallicity assumed. Stellar masses, per the 800 Myr isochrone are indicated. The inset in (b) shows the MS turn-off with B and V photometry.

With a photometric mass of $115^{+5}_{-3} M_\odot$, we compute the tidal radius of Coma Ber as 6.9 ± 0.1 pc, which agrees with the values given by Casewell et al. (2006) (6.5 pc) and Kraus & Hillenbrand (2007) (6.8 ± 0.3 pc). We consider that stars within the tidal radius are bound member candidates (see Table 1), while stars outside belong to the tidal tails. The tidal tail at $X > -8300$ pc (toward Galactic center) and $Y > 0$ is leading and the other tail at $X < -8300$ pc and $Y < 0$ is trailing (Figure 4 (a)).

We redetermine the center of Coma Ber as the mean position of member candidates within the tidal radius to be R.A. = 186.8110 deg and decl. = 25.8112 deg. These are different from those provided by Dias et al. (2014) (R.A. = 186.25 deg, decl. = 26.1 deg). With the average distance of 85.8 pc again obtained from member candidates within the tidal radius, the corresponding Cartesian Galactocentric coordinates are $(X, Y, Z) = (-8305.6, -5.9, +112.3)$ pc. The following analysis is based on the revised cluster center.

For group-X, we obtain a tidal radius of $6.8^{+0.3}_{-0.2}$ pc. However, due to its irregular morphology, determining its center is not straightforward. For simplification, we define its center as the mean position of all member candidates to be R.A. = 217.5175 deg, decl. =

55.0510 deg, and a distance of 101.2 pc, or $(X, Y, Z) = (-8307.2, +55.3, +109.9)$ pc. This center lies in the gap between the two clumps and is a rough estimation. The clumpy shape of group-X suggests the whole system is at a final stage of disruption, since a bound and longer-lived structure should be roundish.

4.4. Dynamical Status

To further quantify the dynamical status of our stellar groups, we compare the photometric mass with the dynamical mass ($M_{dyn,tid}$) for stars within the tidal radius; i.e., these stars are considered to be bound. Due to the irregular morphology of group-X, we do not estimate the dynamical mass of group-X.

The dynamical mass calculated by,

$$M_{dyn} \sim \frac{r_t \sigma_{3D}^2}{G}, \quad (2)$$

(Fleck et al. 2006) where r_t is the 3D tidal radius, and σ_{3D} is the 3D velocity dispersion. Assuming an isotropic velocity distribution within the tidal radius, σ_{3D}^2 is 3 times the 1D velocity dispersion σ^2 estimated from the PM. The resulted $M_{dyn,tid}$ of Coma Ber is in the range $185 M_\odot$ to $375 M_\odot$ ($\sigma_{\mu_\alpha \cos \delta} = 0.20$ km s $^{-1}$, $\sigma_{\mu_\delta} = 0.28$ km s $^{-1}$ by adopting individual distance of

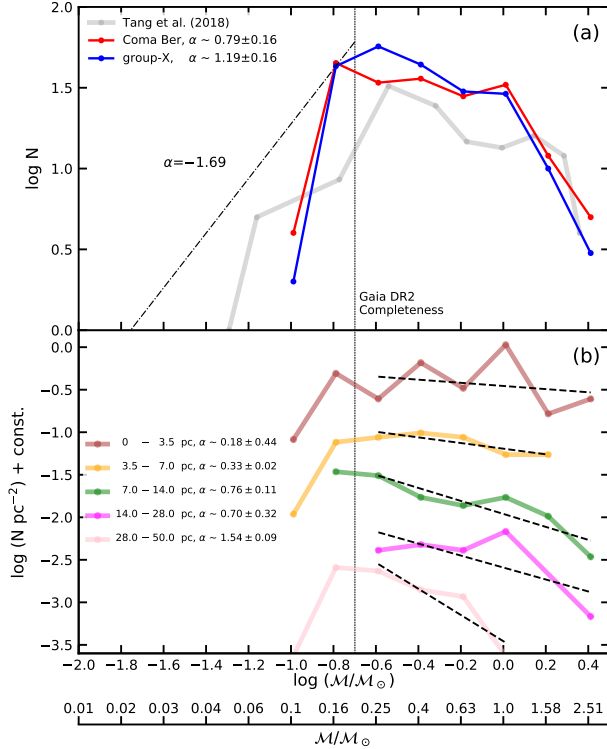


Figure 6. The present day mass function of Coma Ber and group-X with mass derived from PARSEC isochrone with an age of 800 Myr and 400 Myr, respectively. (a): MFs of Coma Ber (red line) and group-X (blue line). The mass function from Tang et al. (2018) for Coma Ber is shown in grey line. The slope, α , is fitted for MF from $0.25 M_\odot$ to $2.51 M_\odot$. (b): surface number density mass functions of Coma Ber in different annuli on the X–Y plane. The slope, α , is fitted with the mass range as the black dashed lines showed. The binwidth is $\log(M/M_\odot)=0.2$. The x-avlue of each dot represents the central value of each bin.

member candidates). Typical error of the 1D proper motion among member candidates is 0.1 mas yr^{-1} , corresponding to 0.04 km s^{-1} , which is much smaller than the measured dispersion within the tidal radius. Compared to the photometric mass within tidal radius $\sim 57 M_\odot$, this is a clear evidence that the cluster is disrupting, which is an interplay between internal and external dynamical evolution.

The major internal dynamical process, two-body relaxation, makes the high-mass stars segregate to the cluster center while low-mass members migrate to the outskirt regions. This process manifests as a change in the slope of the cluster MF in different annuli (Vesperini et al. 2010; Webb & Leigh 2015). As can be seen in Figure 6 (b), the slope of radial MF becomes steeper as the radius increases, confirming the mass segregation as discussed in Section 3.1. Majority of low-mass member

Table 3. Anisotropy of Coma Ber

Annuli (pc)	σ_T (km/s)	σ_R (km/s)	$\frac{\sigma_T}{\sigma_R}$ (4)
(1)	(2)	(3)	(4)
0.0 — 3.5	0.28	0.27	1.06
3.5 — 7.0	0.29	0.29	0.99
7.0 — 14.0	0.40	0.32	1.20
14.0 — 28.0	0.45	0.48	0.95
28.0 — 50.0	1.08	0.95	1.13

NOTE— σ_T and σ_R is the projected tangential and radial velocity dispersion in Coma Ber.

candidates are located in the tidal tails, the outer extended region. Eventually, these stars will expand and become unbound, being stripped away by the external tidal force.

With 3D motions (combining PM and RV), we are able to look for the tidal dissolution in Coma Ber. We use the new cluster center (Section 4.3) and mean velocity within tidal radius as the reference frame, and present the relative 3D velocity in Figure 7 (a) and (b). As can be seen, expansion is not obvious for the bound stars within tidal radius, but only significant at tidal tail regions. Tidal-tail stars are influenced by the Galactic tides and moving away from the cluster center toward the outskirt, which is a clear evidence of dissolution (Portegies Zwart et al. 2001). Similarly, member candidates of the disrupted group-X also exhibit an overall expansion (blue arrows in Figure 7 (a) and (b)).

The existence of expansion in Coma Ber may generate anisotropy in the velocity field. We compute the projected tangential σ_T and radial σ_R velocity dispersions (mean cluster motion subtracted) within different annuli and present them in Table 3. $\sigma_T/\sigma_R = 1$ implies isotropic velocity distribution. Simulations have shown that initially isotropic star cluster will develop anisotropy as a result of two-body relaxation ($\sigma_T/\sigma_R < 1$; Tiongco et al. 2016) or tidal field ($\sigma_T/\sigma_R > 1$; Spurzem & Aarseth 1996; Baumgardt & Makino 2003; Hurley & Shara 2012), in which radial and tangential velocity is dominant respectively. As shown in Table 3, velocity distribution is generally isotropic inside the tidal radius, confirming our assumption for equation (2). A weak tangential anisotropy is found in tidal tail regions, which might be explained by the loss of unbound stars expanding to the Galactic field (Lee et al. 2006).

4.5. Past Encounters and Future Flyby

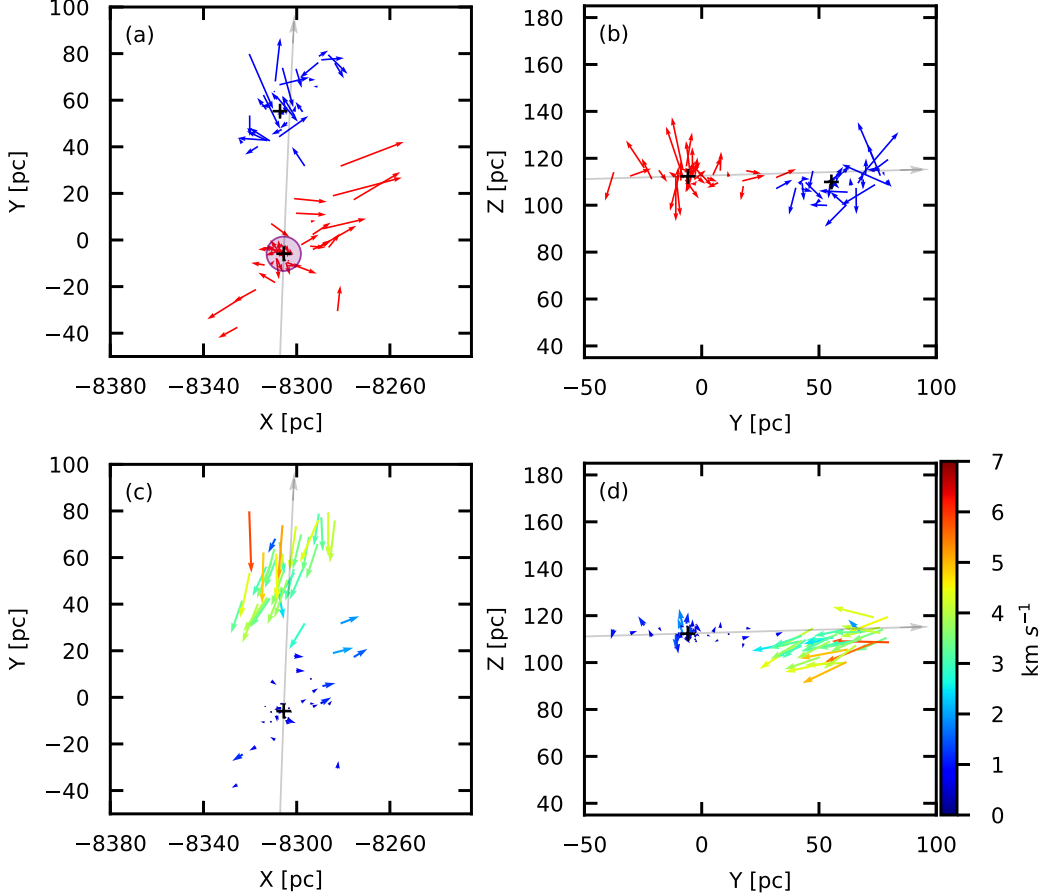


Figure 7. The relative velocity vectors for member candidates in Coma Ber and group-X. (a) The red vectors represent the relative velocity of member candidates of Coma Ber to its mean motion, $(U, V, W)=(8.6, 226.6, 6.8)$ km s^{-1} on the X–Y plane, and the blue vectors the relative velocity of member candidates of group-X to its mean motion, $(U, V, W)=(7.7, 223.2, 5.8)$ km s^{-1} ; Only stars within 1 sigma from the mean value are shown in (a) and (b). The plus sign shows the center of each group (Section 4.3). Purple circle denotes the tidal radius of Coma Ber. (b) the same relative velocity distribution of Coma Ber and group-X on Z–Y plane. (c) The relative velocity distributions of Coma Ber and group-X to the mean motion of Coma Ber on the X–Y plane; (d) the same relative velocity distribution of Coma Ber and group-X on Z–Y plane. The vector length and color coding are scaled to the relative velocity. An integrated orbit the same as the Figure 4 is shown as well.

In Figure 7, the spatial motions of group-X relative to the center of Coma Ber is presented in panel (c) and (d). Stars in group-X are moving toward the Coma Ber center at a speed of 4–6 km s^{-1} . Considering the separation of 65 pc between group-X and the Coma Ber, they may flyby each other in 10–16 Myr (Gavagnin et al. 2016). The irregular clumpy shape of group-X cannot be formed purely due to the tidal interaction with Coma Ber, which is not strong enough. Instead, past close encounters might be the cause. To justify this hypothesis, we estimate the encounter rate in the solar neighborhood. The encounter rate for stellar structures depends on the volume density, geometric cross-section of a cluster and velocity dispersion among clusters (Dieball et al. 2002). In the solar neighbourhood within 200 pc, there are 20 stellar structures with more than 10 members,

and 42 with more than 5 (Oh et al. 2017). We measure their velocity dispersion with U, V, W velocities provided by Gaia DR2 in the range of 11–15 km s^{-1} , and adopt a typical cluster radius of 10 pc (Dieball et al. 2002). The encounter timescale ranges from a few hundreds Myr up to 1 Gyr. It shall be an upper limit due to the incompleteness of (Oh et al. 2017). For a more extended structure, encounter rate shall increase and encounter timescale decrease. We suspect that originally group-X might occupy a larger volume than Coma Ber, thereby experienced more encounters and disrupted into its current morphology. A significant amount of mass-loss must have happened to group-X.

5. SUMMARY

Utilizing the high-precision *Gaia* DR2 astrometry, we apply a new cluster finding method, STARGO, to identify stellar structures around the Coma Ber in the 5-D phase space of $(X, Y, Z, \mu_\alpha \cos \delta, \mu_\delta)$. Additionally to the previously published member candidates of Coma Ber, here we identify for the first time, a leading and a trailing tidal tails of Coma Ber, which extend ~ 50 pc from the cluster center, seven times longer than cluster tidal radius, ~ 6.9 pc.

1. The stars located in the tidal tails of Coma Ber (120) outnumber those inside the tidal radius (77 stars). Member stars inside the tidal radius has an average distance of 85.8 pc, with the center at R.A.= 186.8110 deg, and decl.= 25.8112 deg, corresponding to a Cartesian Galactocentric coordinates of $(X, Y, Z) = (-8305.6, -5.9, +112.3)$ pc.
2. Coma Ber has an age of 700–800 Myr. It has a mass-function slope of $\alpha \sim 0.79 \pm 0.16$ for members from $0.25 M_\odot$ to $2.51 M_\odot$, and a total cluster mass of $\sim 115_{-3}^{+5} M_\odot$.
3. Prominent mass segregation is seen among member candidates, but no obvious expansion is found among stars within the tidal radius of Coma Ber. However, significant expansion is seen in the tidal tails, with a weak anisotropy. Coma Ber is disrupting by losing stars into the Galactic field.
4. A neighboring group, group-X, is re-discovered with 10 times more member candidates than previously known. Group-X is about 65 pc away from Coma Ber. With a comparable number of member candidates as Coma Ber (197), group-X (218) is 400 Myr younger, a steeper slope for the mass function $\alpha \sim 1.19 \pm 0.16$, for stars from $0.25 M_\odot$ to $2.51 M_\odot$.
5. Group-X, with its irregular morphology, is near the end of disruption. It has the center of R.A. = 217.5175 deg, decl. = 55.0510 deg, and a heliocentric distance of 101.2 pc, and $(X, Y, Z) = (-8307.2, +55.3, +109.9)$ pc.

6. Relative motion between both groups suggests a possible fly-by in the next 10–16 Myr.

S.Y.T. and W.P.C. acknowledge the financial support of the grants MOST 106-2112-M-008-005-MY3 and MOST 105-2119-M-008-028-MY3. S.Y.T. also express his gratitude to the financial support of the summer internship at the Max Planck Institute for Astronomy in 2018. X.Y.P. is grateful to the financial support of two grants of National Natural Science Foundation of China, No: 11503015 and 11673032. This study was supported by Sonderforschungsbereich SFB 881 “The Milky Way System” (sub-project B2, B5, and B7) of the German Research Foundation (DFG). Z.Y. is partly supported by the National Key Basic Research and Development Program of China (No. 2018YFA0404501) and NSFC grant 11673083, the Special Funding for Advanced Users through LAMOST FELLOWSHIP. B.S. is a fellow of the International Max Planck Research School for Astronomy and Cosmic Physics at the University of Heidelberg (IMPRS-HD), and acknowledges the support of the Volkswagen Foundation under the Trilateral Partnerships grant 90411, and the PCF program BR05236322. C.C.L. acknowledge the financial support of the grants MOST 106-2917-I-564-042.

We are grateful to Prof. Dr. Chenggang Shu and Prof. Dr. Zhengyi Shao for an in-depth discussion, and to Dr. Shiyin Shen for suggestion on the collaboration. We thank the referee for providing helpful suggestions and comments that improved the quality of the paper. This work made use of data from the European Space Agency (ESA) mission *Gaia* (<https://www.cosmos.esa.int/gaia>), processed by the *Gaia* Data Processing and Analysis Consortium (DPAC, <https://www.cosmos.esa.int/web/gaia/dpac/consortium>). This study also made use of the SIMBAD database and the VizieR catalogue access tool, both operated at CDS, Strasbourg, France.

Software: Astropy (Astropy Collaboration et al. 2013, 2018), galpy (Bovy 2015)

REFERENCES

- Astropy Collaboration, Robitaille, T. P., Tollerud, E. J., et al. 2013, *A&A*, 558, A33
- Astropy Collaboration, Price-Whelan, A. M., Sipőcz, B. M., et al. 2018, *AJ*, 156, 123
- Bailer-Jones, C. A. L., Rybizki, J., Foesneanu, M., Mantelet, G., & Andrae, R. 2018, *AJ*, 156, 58
- Baumgardt, H., & Makino, J. 2003, *MNRAS*, 340, 227
- Bastian, N., Covey, K. R., & Meyer, M. R. 2010, *ARA&A*, 48, 339
- Bonatto, C., Kerber, L. O., Bica, E., & Santiago, B. X. 2006, *A&A*, 446, 121
- Bovy, J. 2015, *The Astrophysical Journal Supplement Series*, 216, 29.
- Bovy, J. 2017, *MNRAS*, 468, L63

- Boss, L. J. 1908, *AJ*, 26, 31
- Bressan, A., Marigo, P., Girardi, L., et al. 2012, *MNRAS*, 427, 127
- Cantat-Gaudin, T., Jordi, C., Vallenari, A., et al. 2018, *A&A*, 618, A93
- Casewell, S. L., Jameson, R. F., & Dobbie, P. D. 2006, *MNRAS*, 365, 447
- Chen, Y., Girardi, L., Bressan, A., et al. 2014, *MNRAS*, 444, 2525
- Chen, Y., Bressan, A., Girardi, L., et al. 2015, *MNRAS*, 452, 1068
- Chen, B., Stoughton, C., Smith, J. A., et al. 2001, *ApJ*, 553, 184.
- Dias, W. S., Monteiro, H., Caetano, T. C., et al. 2014, *A&A*, 564, A79.
- Dieball, A., Müller, H., & Grebel, E. K. 2002, *A&A*, 391, 547
- Dobbie, P. D., Casewell, S. L., Burleigh, M. R., & Boyce, D. D. 2009, *MNRAS*, 395, 1591
- Ernst, A., Just, A., Berczik, P., & Olczak, C. 2011, *A&A*, 536, A64
- Evans, D. W., Riello, M., De Angeli, F., et al. 2018, *A&A*, 616, A4.
- Faherty, J. K., Bochanski, J. J., Gagné, J., et al. 2018, *ApJ*, 863, 91
- Fleck, J.-J., Boily, C. M., Lançon, A., & Deiters, S. 2006, *MNRAS*, 369, 1392
- Gaia Collaboration, Brown, A. G. A., Vallenari, A., et al. 2018, *A&A*, 616, A1
- Gaia Collaboration, van Leeuwen, F., Vallenari, A., et al. 2017, *A&A*, 601, A19
- Gavagnin, E., Mapelli, M., & Lake, G. 2016, *MNRAS*, 461, 1276
- Gillessen, S., Eisenhauer, F., Trippe, S., et al. 2009, *ApJ*, 692, 1075.
- Girven, J., Gänsicke, B. T., Steeghs, D., et al. 2011, *MNRAS*, 417, 1210.
- Griffin, R. E. M., & Griffin, R. F. 2011, *Astronomische Nachrichten*, 332, 105
- Hillenbrand, L. A., & Hartmann, L. W. 1998, *ApJ*, 492, 540
- Høg, E., Fabricius, C., Makarov, V. V., et al. 2000, *A&A*, 355, L27.
- Hurley, J. R., & Shara, M. M. 2012, *MNRAS*, 425, 2872
- Kerr, F. J., & Lynden-Bell, D. 1986, *MNRAS*, 221, 1023
- Kraus, A. L., & Hillenbrand, L. A. 2007, *AJ*, 134, 2340
- Kruijssen, J. M. D. 2012, *MNRAS*, 426, 3008
- Lada, C. J., & Lada, E. A. 2003, *ARA&A*, 41, 57
- Lee, K. H., Lee, H. M., & Sung, H. 2006, *MNRAS*, 367, 646
- Lindgren, L., Hernández, J., Bombrun, A., et al. 2018, *A&A*, 616, A2
- Maíz Apellániz, J., & Weiler, M. 2018, *A&A*, 619, A180
- Martinez-Medina, L. A., Pichardo, B., Peimbert, A., & Moreno, E. 2017, *ApJ*, 834, 58
- Meingast, S., & Alves, J. 2019, *A&A*, 621, L3
- Melnikov, S., & Eislöffel, J. 2012, *A&A*, 544, A111
- Melotte, P. J. 1915, *MmRAS*, 60, 175
- Mermilliod, J.-C., Grenon, M., & Mayor, M. 2008, *A&A*, 491, 951
- Odenkirchen, M., Soubiran, C., & Colin, J. 1998, *NewA*, 3, 583
- Odenkirchen, M., Grebel, E. K., Rockosi, C. M., et al. 2001, *ApJL*, 548, L165
- Odenkirchen, M., Grebel, E. K., Dehnen, W., et al. 2003, *AJ*, 126, 2385
- Oh, S., Price-Whelan, A. M., Hogg, D. W., Morton, T. D., & Spergel, D. N. 2017, *AJ*, 153, 257
- Pang, X., Grebel, E. K., Allison, R. J., et al. 2013, *ApJ*, 764, 73
- Pinfield, D. J., Jameson, R. F., & Hodgkin, S. T. 1998, *MNRAS*, 299, 955
- Piskunov, A. E., Schilbach, E., Kharchenko, N. V., Röser, S., & Scholz, R.-D. 2008, *A&A*, 477, 165
- Portegies Zwart, S. F., McMillan, S. L. W., Hut, P., & Makino, J. 2001, *MNRAS*, 321, 199
- Reid, M. J., & Brunthaler, A. 2004, *ApJ*, 616, 872
- Robin, A., Reylé, C., Derrière, S., and Picaud, S., 2003, *A&A*, 409
- Röser, S., Schilbach, E., & Goldman, B. 2019, *A&A*, 621, L2
- Rybizki, J., Demleitner, M., Fouesneau, M., et al. 2018, *PASP*, 130, 74101.
- Schönrich, R., Binney, J., & Dehnen, W. 2010, *MNRAS*, 403, 1829.
- Sharma, S., Bland-Hawthorn, J., Johnston, K. V., and Binney, J., 2011, *ApJ*, 730, 3
- Spitzer, L., Jr. 1958, *ApJ*, 127, 17
- Spitzer, L. 1987, Princeton, NJ, Princeton University Press, 191
- Spurzem, R., & Aarseth, S. J. 1996, *MNRAS*, 282, 19
- Tadross, A. L., Werner, P., Osman, A., & Marie, M. 2002, *NewA*, 7, 553
- Tang, J., Bressan, A., Rosenfield, P., et al. 2014, *MNRAS*, 445, 4287
- Tang, S.-Y., Chen, W. P., Chiang, P. S., et al. 2018, *ApJ*, 862, 106
- Tiongco, M. A., Vesperini, E., & Varri, A. L. 2016, *MNRAS*, 455, 3693
- Trumpler, R. J. 1938, *Lick Observatory Bulletin*, 18, 167
- Urban, S. E., Corbin, T. E., & Wycoff, G. L. 1998, *AJ*, 115, 2161

- Vesperini, E., McMillan, S. L. W., D'Antona, F., & D'Ercole, A. 2010, *ApJL*, 718, L112
- Webb, J. J., & Leigh, N. W. C. 2015, *MNRAS*, 453, 3278
- Weiler, M. 2018, *A&A*, 617, A138
- Wu, Y., Du, B., Luo, A., Zhao, Y., & Yuan, H. 2014, *Statistical Challenges in 21st Century Cosmology*, 306, 340
- Wu, Y., Luo, A., Du, B., & Guo, Y. 2014, *Setting the scene for Gaia and LAMOST*, 298, 445
- Yang, S.-C., Sarajedini, A., Deliyannis, C. P., et al. 2013, *ApJ*, 762, 3
- Yuan, Z., Chang, J., Banerjee, P., et al. 2018, *ApJ*, 863, 26
- Zuckerman, B., & Song, I., 2004, *ARA&A*, 42, 685

APPENDIX

A. COORDINATE SYSTEM DEFINITIONS

The Galactocentric coordinates used in this study have a positive x direction pointing from the position of the Sun projected to the Galactic mid-plane to the Galactic center (GC) (approximately where $l = 0$ and $b = 0$); the y -axis points towards $l = 90^\circ$; the z -axis roughly points towards $b = 90^\circ$. Other parameters are listed below:

1. GC coordinates (ICRS) (Reid & Brunthaler 2004):
 - (a) R.A. = $17^{\text{h}}45^{\text{m}}37^{\text{s}}.224$
 - (b) decl. = $-28^\circ56'10''.23$
2. Distance to the GC = 8.3 kpc (Gillessen et al. 2009)
3. Distance of the Sun above the Galactic mid-plane = 27 pc (Chen et al. 2001)
4. Solar motion relative to the GC (Schönrich et al. 2010; Bovy 2015):

$$(U, V, W) = (+11.10, +232.24, +7.25) \text{ km s}^{-1}$$